

# Broad emission lines for a negatively spinning black hole

T. Dauser<sup>1\*</sup>, J. Wilms<sup>1</sup>, C.S. Reynolds<sup>2</sup>, and L.W. Brenneman<sup>3</sup>

<sup>1</sup> *Dr. Karl Remeis-Observatory and Erlangen Centre for Astroparticle Physics, Sternwartstr. 7, 96049 Bamberg, Germany*

<sup>2</sup> *Department of Astronomy and Maryland Astronomy Center for Theory and Computation, University of Maryland, College Park, MD 20742, USA*

<sup>3</sup> *Harvard-Smithsonian Center for Astrophysics, 60 Garden Street, Cambridge, MA 02138, USA*

29 May 2018

## ABSTRACT

We present an extended scheme for the calculation of the profiles of emission lines from accretion discs around rotating black holes. The scheme includes discs with angular momenta which are parallel and antiparallel with respect to the black hole’s angular momentum, as both configurations are assumed to be stable. We discuss line shapes for such discs and present a code for modelling observational data with this scheme in X-ray data analysis programs. Based on a Green’s function approach, an arbitrary radius dependence of the disc emissivity and arbitrary limb darkening laws can be easily taken into account, while the amount of precomputed data is significantly reduced with respect to other available models.

**Key words:** Accretion, Accretion Discs, black hole physics, Galaxies: Nuclei, galaxies: active, Lines: Profiles

## 1 INTRODUCTION

Skew-symmetric, broadened Fe  $K\alpha$  emission lines are seen in many Active Galactic Nuclei (AGN) such as MCG–6-30-15 (Tanaka et al. 1995; Wilms et al. 2001; Miniutti et al. 2007), 1H0707–495 (Fabian et al. 2009), and others (Nandra et al. 2007), Galactic black hole binaries such as Cygnus X-1 (Fabian et al. 1989; Miller et al. 2002), GX 339–4 (Miller et al. 2004; Caballero-García et al. 2009), or GRS 1915+105 (Martocchia et al. 2002; Blum et al. 2009), and neutron star systems (di Salvo et al. 2009; Cackett et al. 2008, 2009; Shaposhnikov et al. 2009). These lines are generally interpreted as being caused by the relativistic motion of the line emitting material close to the central compact object. Since the line shape depends on the spin of the black hole,  $a$ , and the emissivity and inclination of the surrounding accretion disc, the diagnostic power of relativistic lines is very high, as they provide one of the most direct ways to probe the physics of the region of strong gravity close to the black hole (see, e.g., Reynolds & Nowak 2003, for a review). High signal-to-noise observations of AGN and Galactic black holes have already resulted in several measurements of  $a$  with formally small error bars (Brenneman & Reynolds 2006; Miller et al. 2004, 2008, 2009), with systematic effects due to the high count rate of Galactic sources (Yamada et al. 2009; Done & Diaz Trigo 2010) and due to the uncertainty of the parameters of the underlying continuum (e.g., Ross & Fabian 2007; Reynolds & Fabian 2008) currently dominating the uncertainty of the measurements.

Observations of AGN in the *XMM-Newton* and *Chandra* deep fields prove that broadened iron lines already occurred at high redshifts,  $z$ , (Comastri et al. 2004; Streblyanska et al. 2005,

but see Corral et al. 2008). Although recent studies seem to exclude that these broad lines are a common feature (Longinotti et al. 2008), observations of such lines could therefore be used to study the expected evolution of black hole spin with  $z$ . For example, strong changes in amplitude and direction for the central black hole are predicted in stochastic evolution models (King et al. 2008; Volonteri et al. 2005). Observations of cavities in nearby galaxy clusters are also evidence for spin evolution (Wise et al. 2007; Fabian et al. 2000). In galactic binary systems, the initial kick during the formation of a stellar-mass black hole in a supernova can lead to a strong misalignment between the disc and the black hole (Brandt & Podsiadlowski 1995).

Depending on the mode of accretion, in all of these scenarios it is possible that the angular momenta of black hole and accretion disc become antiparallel, i.e., the black hole has “negative spin”. As shown by King et al. (2005), both parallel and antiparallel alignments of the disc and black hole angular momenta are stable configurations; misaligned discs will evolve to one of them. It is therefore not unlikely that a configuration with antiparallel spins exists in nature. In fact, accretion onto rapidly-spinning retrograde black holes may be of some importance for understanding the properties of powerful radio-loud AGN. Employing the flux-trapping model of Reynolds et al. (2006), Garofalo (2009) argues that an accretion disk around a retrograde black hole is a particularly potent configuration for generating powerful jets. Moreover this might also explain the lack of radio-loud AGN in observations (Garofalo et al. 2010). It is tantalizing that the broad iron line in the powerful radio-loud AGN 3C120 implies a truncation at  $r \sim 10 GM/c^2$  (Kataoka et al. 2007), very close to the innermost stable circular orbit (ISCO) for a rapidly-rotating retrograde black hole. However, a further exploration of this line of thought requires fully-relativistic iron line models that are valid for retrograde black

\* E-mail: thomas.dauser@sternwarte.uni-erlangen.de

holes. Although first calculations of line profiles for a negatively spinning black hole were already performed, e.g., by Jaroszynski (1997) and Schnittman (2006), none of the currently available models for relativistic lines such as `diskline` (Fabian et al. 1989), `laor` (Laor 1991), `kerrdisk` (Brenneman & Reynolds 2006), or the `ky`-family of models (Dovčiak et al. 2004) are valid for black holes with retrograde accretion discs.

In this *Paper* we therefore extend the formalism of Cunningham (1975) employed by many of these models to the case of  $-0.998 \leq a \leq +0.998$ . Section 2 presents an overview of the scheme used for the calculations, including a new approach which reduces significantly the amount of data to be precalculated and allows for a flexibility in terms of the emissivity of the accretion disc and the limb-darkening law (Sect. 2.4). The implementation of this scheme in a new code for calculating relativistic lines, `relline`, and the comparison of this scheme with other models is described in Sect. 2.5. Section 3 presents results for line profiles and summarizes our results.

## 2 THEORY: RELATIVISTICALLY BROADENED LINES

### 2.1 The equations of motion around a rotating black hole

In order to account for the strongly curved space and allow a spinning black hole, a fully relativistic approach in the Kerr (1963) metric was chosen. This metric is characterized by the mass,  $M$ , and the angular momentum,  $J$ , of the black hole, which is commonly parametrized as  $a = J/M$ . We will call the black hole in a system where it spins in the opposite direction of the accretion disc a *negatively spinning* black hole (i.e.  $a < 0$ ). Throughout this paper, units of  $G \equiv c \equiv 1$  are chosen. The line element in Boyer & Lindquist (1967) coordinates is

$$ds^2 = -\left(1 - \frac{2Mr}{\Sigma}\right) dt^2 - \frac{4aMr \sin^2 \theta}{\Sigma} dt d\varphi + \Sigma \Delta dr^2 + \Sigma d\theta^2 + \left(r^2 + a^2 + \frac{2a^2 Mr \sin^2 \theta}{\Sigma}\right) \sin^2 \theta d\varphi^2, \quad (1)$$

where  $\Delta = r^2 - 2Mr + a^2$  and  $\Sigma = r^2 + a^2 \cos^2 \theta$ , the angle  $\phi$  is measured in the plane of the disc, and the black hole's angular momentum points towards  $\theta = 0$ . Taking into account the black hole's interaction with thermal photons from the accretion disc, its spin is restricted to  $a \leq a_{\max} < 1$  as capturing photons with negative angular momentum (with respect to the movement of the disc) becomes more likely for increasing  $a$  and thus prevents a spin up to the extreme value of  $a = 1$  (Thorne 1974). Assuming that a negatively spinning system is created by flipping the spin of a system with  $a > 0$  sets the lower limit of the spin at  $a \geq -a_{\max}$ , as infalling matter from the counterrotating disc clearly decreases the absolute value of the spin with time. We choose  $a_{\max} = 0.998$ , which is commonly used and has been calculated by Thorne (1974).

As we are interested in particle orbits around the black hole, we need to derive the equations of motion for a test particle in the Kerr metric. This can, e.g., be done by solving the Geodesic equation directly, which formally is a general equation of motion for all possible metrics in General Relativity. Using the conserved quantities of motion (Carter 1968), i.e., the energy  $E$ , the angular momentum  $L$ , the rest mass  $\mu$  of the particle, and

$$\mathcal{Q} = p_\theta^2 + \cos^2 \theta \left[ a^2 (\mu^2 - p_t^2) + p_\varphi^2 / \sin^2 \theta \right] \quad (2)$$

the general equations of motion are (Bardeen et al. 1972):

$$\Sigma \dot{t} = -a(aE \sin^2 \theta - L) + (r^2 + a^2) \frac{T}{\Delta} \quad (3)$$

$$\Sigma \dot{r} = \pm \sqrt{V_r} \quad (4)$$

$$\Sigma \dot{\theta} = \pm \sqrt{V_\theta} \quad (5)$$

$$\Sigma \dot{\varphi} = -\left(aE - \frac{L}{\sin^2 \theta}\right) + a \frac{T}{\Delta}, \quad (6)$$

where

$$V_r = T^2 - \Delta (\mu^2 + r^2 + (L - aE)^2 + \mathcal{Q}), \quad (7)$$

$$V_\theta = \mathcal{Q} - \cos^2 \theta (L^2 / \sin^2 \theta + a^2 (\mu^2 - E^2)) \quad (8)$$

and

$$T = E(r^2 + a^2) - aL. \quad (9)$$

The signs in Eq. 4 and Eq. 5 can be chosen independently and account for the direction of the photon. The upper sign means a movement with growing  $r/\theta$  and the lower sign stands for the opposite behaviour, respectively. Thus they can be chosen arbitrarily, but change, e.g., when a turning point occurs.

### 2.2 The accretion disc

For simplicity we assume a geometrically thin accretion disc which lies in the equatorial plane of the system, i.e.,  $\theta = \pi/2$  and  $\dot{\theta} = 0$ . Additionally we require the disc to be stationary and to consist of particles orbiting the compact object on circular orbits. This approach fully determines the system (Bardeen et al. 1972). Taking into account that the particles can be on pro- and retrograde orbits with respect to the spinning direction of the black hole, the particles have an angular velocity

$$\omega = \frac{\sqrt{M}}{r\sqrt{r} + a\sqrt{M}}. \quad (10)$$

The four-velocity of the accretion disc is given by

$$u^\mu = u^t (\partial_t + \omega \partial_\phi) \quad (11)$$

where

$$u^t = \frac{r\sqrt{r} + a\sqrt{M}}{\sqrt{r}\sqrt{r^2 - 3Mr + 2a\sqrt{M}\sqrt{r}}}. \quad (12)$$

Further calculation reveals (Bardeen et al. 1972) that there exists a radius of *marginal stability* (often referred to as innermost stable circular orbit, ISCO) at

$$r_{\text{ms}}(a) = M \left( 3 + Z_2 - \text{sgn}(a) \sqrt{(3 - Z_1)(3 + Z_1 + 2Z_2)} \right), \quad (13)$$

where

$$Z_1 = 1 + (1 - a^2)^{1/3} \left[ (1 + a)^{1/3} + (1 - a)^{1/3} \right] \quad (14)$$

and

$$Z_2 = \sqrt{3a^2 + Z_1^2}. \quad (15)$$

Thus the inner edge of the accretion disc has to be at a radius  $r_{\text{in}} > r_{\text{ms}}$ , as no stable circular orbits can exist inside of it. The minimum inner radius of an accretion disc is  $r_{\text{ms}}(a = +0.998) = 1.23 r_g$ , where  $r_g = GM/c^2$  is called gravitational radius. This orbit is only possible for particles circulating around a maximally rotating black hole with positive angular momentum, as the orbits are supported by frame-dragging effects. In the case of a negative spin, the same effects push the inner edge out to  $r_{\text{ms}}(a = -0.998) \sim 9 r_g$ .

### 2.3 Radiation transport

Having described the accretion disc, i.e. the frame where the photons are emitted, we can now trace them back to a distant observer. Following, e.g., Krolik (1999), we use the effective Lagrangian

$$\mathcal{L}_{\text{eff}} = \frac{1}{2} g_{\mu\nu} \dot{x}^\mu \dot{x}^\nu \quad (16)$$

for massless particles ( $\mu = 0$ ) in order to calculate the photon's momentum

$$p_\mu = d\mathcal{L}/dx^\mu = E \left( -1, \pm 1/\Delta\sqrt{V_r}, \pm\sqrt{V_\theta}, \lambda \right)^T \quad (17)$$

where  $E$  is the energy of the photon in flat space and thus in very good approximation the photon's energy measured by an observer at large distance.  $\lambda = L/E^2$  can be interpreted as the angular momentum.

As the photons originate from a stationary and axi-symmetric accretion disc, we only have to consider the motion in  $(r, \theta)$  direction. Using the equations of motion (Eq. 3 - 6), this assumption reduces the problem of determining the trace of a photon to solving

$$\int_{r_e}^{\infty} \frac{dr}{\sqrt{V_r}} = \int_{\pi/2}^{\theta_o} \frac{d\theta}{\sqrt{V_\theta}} \quad (18)$$

where the integration is carried out from the point of emission  $(r, \theta) = (r_e, \pi/2)$  to the observer at  $(\infty, \theta_o)$  (Carter 1968). Here  $r_e$  is the radius of emission and  $\theta_o$  the angle with respect to the normal of the accretion disc at which the photon is observed. Note that solving Eq. 18 fully determines all constants of motion and thus the momentum and therefore the emission angle of the photon,  $\theta_e$ , is fixed. By splitting the integral into parts and keeping track of the correct sign in front of  $\sqrt{V_r}$  and  $\sqrt{V_\theta}$  (see Sec. 2.1), turning points in  $r$  and  $\theta$  direction can be taken into account.

To calculate the specific intensity  $I_E^{\text{obs}}(\theta_o)$  observed under the angle  $\theta_o$  at energy  $E$ , we have to integrate over the local specific intensity  $I_{E_e}(r_e, \theta_e)$  emitted from the accretion disc. As the direction of a photon changes along its way to the observer due to strong gravity, as shown by Cunningham & Bardeen (1973) this integration is easily performed after the disc is projected onto a plane perpendicular to the line of sight, spanned by the impact parameters  $\alpha$  and  $\beta$ , which are connected to the solid angle through (Cunningham & Bardeen 1973)

$$d\alpha d\beta = D^2 d\Omega \quad , \quad (19)$$

where  $D$  is the distance to the observer. In order to obtain the specific intensity on the projected plane, we use Liouville's theorem,  $I_E/E^3 = \text{const.}$  (Lindquist 1966). Integrating over the projected accretion disc then yields

$$I_E^{\text{obs}}(\theta_o) = \int \left( \frac{E}{E_e} \right)^3 I_{E_e}(r_e, \theta_e) d\alpha d\beta \quad . \quad (20)$$

We define the general relativistic Doppler shift  $g = E/E_e$ , which can be calculated from the four-velocity of the accretion disc (Eq. 12) and the momentum of the photon (Eq. 17) (Cunningham 1975),

$$g = \frac{E}{E_e} = -\frac{p^t}{p_e^\mu u_\mu} = \frac{\sqrt{r_e} \sqrt{r_e^2 - 3Mr_e + 2a\sqrt{Mr_e}}}{r_e \sqrt{r_e} + a\sqrt{M} - \sqrt{M}\lambda} \quad . \quad (21)$$

Note that for the special case of viewing the accretion disc from top ( $\theta_o=0$ , leading to  $\lambda = 0$ ), the purely gravitational redshift for a negative spin is slightly higher than for positive  $a$ . Figure 1 shows

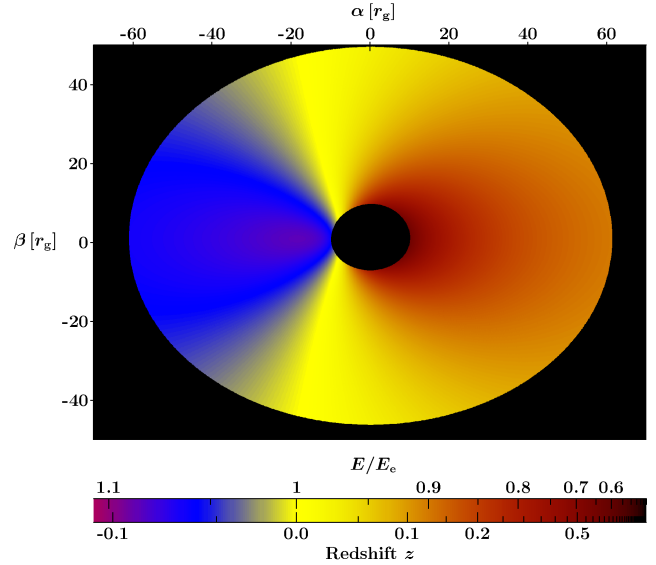


**Figure 1.** Map of a retrograde accretion disc around a maximally spinning black hole ( $a = -0.998$ ) as seen from a distant observer at an inclination angle of  $\theta_o = 40^\circ$ . The disc truncates at  $60 r_g$ .  $\alpha$  and  $\beta$  are the coordinates defined on the plane of the sky (i.e., perpendicular to the line of sight; see Eq. 19). The color code shows the energy shift of the photons, asymmetries are due to relativistic light bending. The blue-shifted left part of the disc moves towards the observer, whereas the right part recedes from the observer.

the redshift of a complete accretion disc as seen by a distant observer, illustrating the effects of gravitational redshifting, Doppler boosting, and light bending.

Using the maximum and minimum energy ratio  $g$  on a certain ring of the accretion disc, following Cunningham (1975) we can additionally define

$$g^* = \frac{g - g_{\min}}{g_{\max} - g_{\min}} \in [0, 1] \quad (22)$$

This approach allows us to perform a coordinate transformation from  $(\alpha, \beta)$  to  $(r_e, g^*)$  and to carry out the integration (Eq. 20) over the accretion disc. The expression for the coordinate transform is commonly simplified further by introducing the *transfer function* (Cunningham 1975)

$$f(g^*, r_e, \theta_o) = \frac{1}{\pi r_e} g \sqrt{g^*(1-g^*)} \left| \frac{\partial(\alpha, \beta)}{\partial(g^*, r_e)} \right| \quad . \quad (23)$$

Note that here the determinant can not be calculated analytically and thus the transfer function has to be evaluated numerically. Using the above equations, the observed intensity under an inclination angle  $\theta_o$  then is

$$I_E^{\text{obs}}(\theta_o) = \int_{r_{\text{in}}}^{r_{\text{out}}} \int_0^1 \frac{\pi r_e g^2 f(g^*, r_e, \theta_e)}{\sqrt{g^*(1-g^*)}} I_{E_e}(r_e, \theta_e) dr dg^* \quad , \quad (24)$$

where the inner and outer radii of the accretion disc are  $r_{\text{in}}$  and  $r_{\text{out}}$ , respectively.

### 2.4 Calculating Relativistic Line Profiles

The effort to calculate line profiles is almost fully buried in the determination of the transfer function, which depends in general on four parameters ( $a, \theta_o, r_e$ , and  $g$ ). In order to allow for a real-time

fitting of observational data it is generally necessary to precalculate  $f$  or some variant of it. The quality of a given model then depends strongly on the amount of precalculated information. Table sizes can amount up to several hundreds of megabytes.

In most available models, the approach chosen is to precalculate the value of the inner integral in Eq. 24 using a Gaussian line shape for  $I_{E_e}$  and some prescription of the limb-darkening law, i.e., the dependence of  $I_{E_e}$  from  $\theta_e$ . A disadvantage of this approach is that any change of the limb-darkening law necessitates a recomputation of the precalculated tables. In order to avoid this problem, we use a Green's function approach to model the specific intensity originating from the disc as purely mono-energetic at  $E_0$ ,

$$I_{E_e}(r_e, \theta_e) = \delta(E_e - E_0) \varepsilon(r_e, \theta_e) \quad , \quad (25)$$

The dependencies of the local intensity on the emission angle  $\theta_e$  (e.g., limb darkening effects) and the radius  $r_e$  are described by  $\varepsilon(r_e, \theta_e)$ . Inserting this into Eq. 24 and evaluating the delta function then gives

$$I_{E_0}^{\text{obs}}(\theta_o) = \int_{r_{\text{in}}}^{r_{\text{out}}} \frac{\pi g^3 r_e f(g^*, r_e, \theta_o)}{E_0 (g_{\text{max}} - g_{\text{min}}) \sqrt{g^*(1-g^*)}} \varepsilon(r_e, \theta_e) dr_e \quad (26)$$

where the transfer function  $f$  can be calculated using the code of Speith et al. (1995).

As the integration over  $r$  is trivial, we focus on the emission of one radius and its contribution  $I_{E_i}^{\text{obs}}(r)$  to a certain energy bin  $i$  ranging from  $E_{i0}$  to  $E_{i1}$ . Using Eq. 26,

$$I_{E_i}^{\text{obs}}(r) \propto \int_{E_{i0}}^{E_{i1}} \frac{g^3 f(g^*)}{(g_{\text{max}} - g_{\text{min}}) \sqrt{g^*(1-g^*)}} dE \quad , \quad (27)$$

where the integrand diverges at  $g^* = 0$  and  $g^* = 1$ , i.e., at the two points on the ring where the minimum and maximum energy shifts occur with respect to  $E_0$ . As the divergences imply that these points contribute significantly to the overall luminosity, great care has to be taken by numerical integration. In order to avoid numerical instabilities, we make use of the fact that the dependence of  $f(g^*)$  close to these points can be calculated analytically as

$$f(g^* \rightarrow 0) \propto \sqrt{1-g^*} \quad \text{and} \quad f(g^* \rightarrow 1) \propto \sqrt{g^*} \quad . \quad (28)$$

This leaves the integrand of Eq. 27 with a divergence of the kind  $1/\sqrt{x}$  for  $x \rightarrow 0$ . Assuming that  $g \sim \text{const.}$  in this energy bin, the integration can be performed analytically, leading to

$$I_{E_i}^{\text{obs}}(r) \propto 2(\sqrt{E_{i1}} - \sqrt{E_{i0}}) \quad . \quad (29)$$

As the above assumption might not be valid for the whole bin, we define a criteria by choosing a sufficiently small value of  $h$  such that it is legitimate to use Eq. 29 for  $g^* \in [0, h]$  and  $g^* \in [1-h, 1]$ . The normalization factors are then determined from  $I_h^{\text{obs}}(r)$  and  $I_{1-h}^{\text{obs}}(r)$ . For  $g^* \in [h, 1-h]$ , an adaptive Romberg method is chosen to solve Eq. 26 directly. These numerical improvements serve to avoid the spikes seen in some other models and keep the advantages of the Green's function approach (see below).

## 2.5 The `relline` Model

We have implemented the formalism of Sect. 2.4 as a model function, called `relline`, that can be added to data analysis software such as ISIS (Houck & Denicola 2000) or XSPEC (Arnaud 1996). In order to reduce the required CPU time, following Brenneman & Reynolds (2006) we calculate the transfer

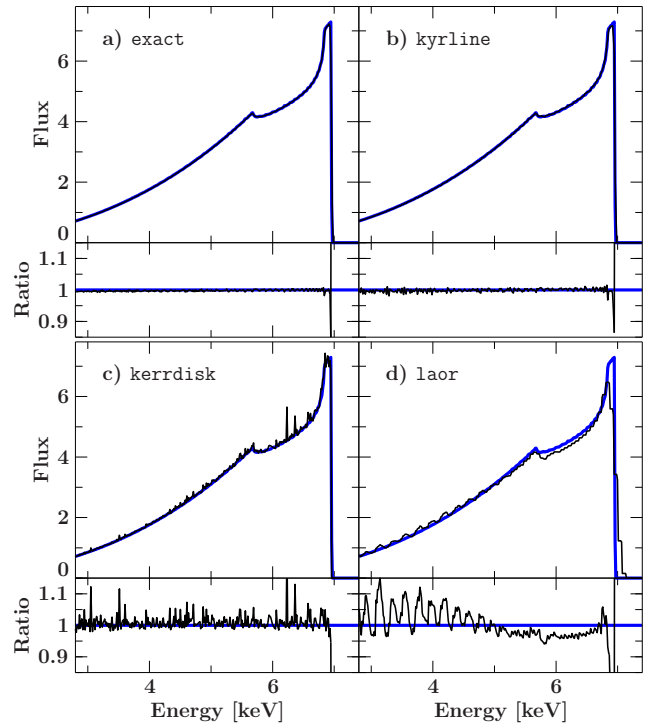


**Figure 2.** Comparison of the `relline` model (blue) with a) the exact line profile, b) `kyrline`-, c) `kerrdisk`- and d) the `laor`-model for an emission line at  $E_0 = 6.4$  keV around a black hole with  $a = +0.998$ , an inclination angle of  $\theta_o = 40^\circ$ , an emissivity  $r^{-3}$ , and an outer radius of  $50 r_g$ .

function (Eq. 23) for various combinations of  $-0.998 \leq a \leq 0.998$  and  $0^\circ \leq \theta \leq 89^\circ$ . The highly resolved line profile is then calculated using a linear interpolation of the slowly varying transfer function followed by a numerical integration over  $r$  for the returned intensity. The `relline` model is provided at [www.sternwarte.uni-erlangen.de/research/relline/](http://www.sternwarte.uni-erlangen.de/research/relline/). Both an additive and a convolution model are provided (the latter for calculating the relativistic smearing of continuum components). The code also provides for several different limb-darkening and limb-brightening laws (see Svoboda et al. 2009 for a discussion of different limb-darkening laws).

Figure 2 shows a comparison of the `relline` model to models commonly used in X-ray astronomy. A comparison of the model with an exact numerical evaluation of Eq. 24 that does not make use of precalculated quantities and interpolation shows that there is no significant deviation between both approaches (Fig. 2a). In addition, for  $a \geq 0$  the produced shape is very similar to the `kyrline` model, which uses a table a factor 10 times larger and a Gaussian emission profile instead of a delta function (Fig. 2b). This result shows that for  $a \geq 0$  and when it is sufficient to use the limb-darkening law of Laor (1991) or the limb-brightening law of Haardt (1993), both models can be used with confidence. For completeness, Fig. 2c and Fig. 2d compare the exact profile to the `kerrdisk` and the `laor` model. Spikes in the former model are due to divergences in the integration of the transfer function (see Sect. 2.5). We note, however, that if the line is evaluated on an energy grid appropriate for a Silicon detector, these spikes will be averaged out and therefore have no effect on any of the published results. The `laor`-model, on the other hand, shows strong deviations from the correct line shape which are caused by the coarse

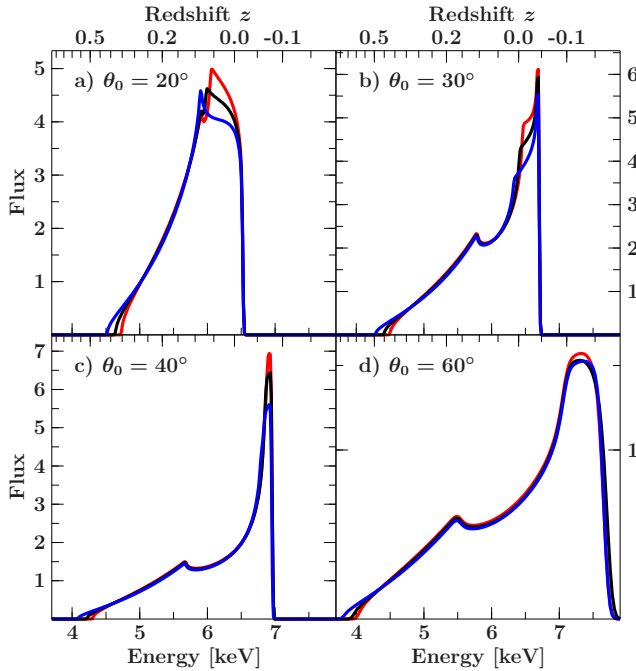


**Figure 3.** Line profiles of a relativistic iron line emitted at 6.4 keV in the rest-frame of the disc. Typical inclination angles  $\theta_0$  are displayed along with an emissivity of  $r^{-3}$ . The maximal spinning black hole ( $a = +0.998$ ) is drawn in red (dashed in the printed version), the non-rotating ( $a = 0$ ) in black (dashed-dotted), and the blue (solid) line shows the broad emission line for maximal negative spin ( $a = -0.998$ ). In order to allow comparison of the line shapes, the inner edge of the accretion disc was set to  $r = 9 r_g$  for all profiles.

energy grid. Especially in the tail of the line these deviations are large enough that they could bias model fitting. For this reason, we caution against using this model in data analysis work.

### 3 DISCUSSION AND CONCLUSIONS

In Figure 3 we compare the line profiles for a maximally rotating Kerr black hole, a Schwarzschild black hole, and a black hole which is maximally counterrotating for several different inclinations. The accretion disc emissivity was assumed to be  $\epsilon \propto r^{-3}$ , i.e., the emissivity obtained from a simple accretion disc in the Newtonian regime. This dependence is assumed in many of the earlier models (e.g., Fabian et al. 1989; Laor 1991). Note that this assumption can be easily dropped in all modern line models. In order to allow for a comparison of the line shapes with earlier results, we use the limb-darkening law of Laor (1991), even though for lines caused by fluorescence due to the irradiation of a disc with hard X-rays from above, a limb-brightening law would be more appropriate (Svoboda et al. 2009). In order to illustrate the pure frame-dragging effects of these different spins onto the line shape, the inner disc radius was set to  $9 r_g$  for all three spins. The Figure shows that in this case the major difference between the different spins is the relative strength of the core of the line to the red wing, which decreases with decreasing  $a$ . For this case of a large inner radius, the most significant differences in line shape are seen for low values of  $\theta_0$  while the red tails are virtually indistinguishable. The slight increase in line flux at the lowest energies is due to the increased Doppler boosting in the case of  $a < 0$  (for a given radius,  $u^t$  increases with decreasing  $a$ , cf. Eq. 12). The difference in energy

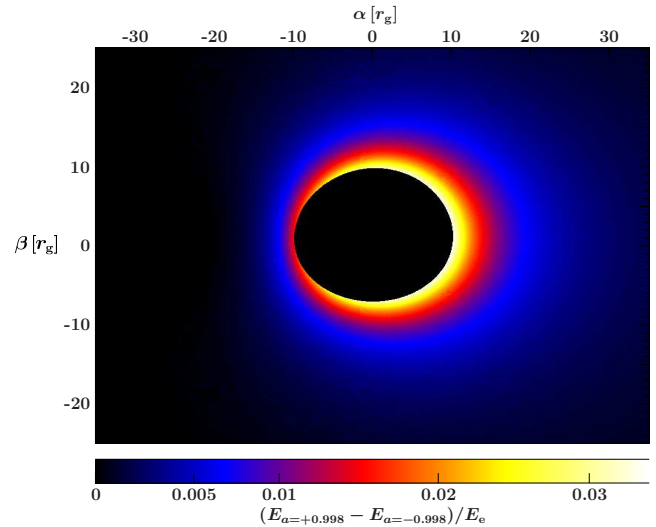


**Figure 4.** Difference between the energy shifts experienced by photons from a maximally positively and a maximally negatively spinning accretion disc with inner radius  $r_{\text{in}} = 9 r_g$ , viewed under an inclination of  $40^\circ$ .

shift of photons emerging from an accretion disc between maximal positive and maximal negative spin of the black hole is shown in Fig. 4. As these differences are highest close to inner edge of the disc, a higher emissivity pronounces the deviations in the line profiles. Moreover this figure shows that for an accretion disc with an inner radius larger than  $30 r_g$  no significant differences would be expected.

Figure 5 shows line profiles for different spins of the black hole for the more realistic case that the disc extends down to the marginally stable orbit. Since the inner edge of the disc is closer to the black hole for positively spinning black holes, more strongly redshifted photons emerge. As already noted by Jaroszynski (1997), this leads to broader lines in these systems, especially for discs with an emissivity that is strongly peaked towards  $r_{\text{in}}$ . Maximally negatively spinning black holes have the smallest width, although the line will still be detectable as being broad even at CCD resolution (depending on inclination, typical widths of the main peak are around 200 eV). Lines from counterrotating black holes will therefore be more difficult to detect than lines from positively rotating black holes.

The major difference of line shapes for discs around black holes with  $a = 0$  and counterrotating discs (see Fig. 5) lies in the strength of the blue peak, since the skew symmetric shape is mainly due to frame dragging effects and the small inner radii. Detecting these lines observationally is therefore more difficult than detecting lines from discs around a positively rotating black hole. In addition, as shown by Svoboda et al. (2009) limb-darkening/-brightening affects the strength of the red wing. For counterrotating black holes, this results in a possible degeneracy, as for different limb-darkening laws similar line shapes might result for  $a \sim 0$  and  $a = -0.998$ . Using a physically motivated limb-darkening law would avoid this degeneracy. The line shapes also become more similar if the assumption that emission down to the radius of marginal stability contributes to the shape is dropped. This assumption might not be justified in some cases, as fluorescent emission only takes place in irradiated parts of the disc which are not fully ionized. Thus the inner radius of the emission becomes larger, which results in a weaker red tail of the line profile. This effect leads to line shapes for different spin that are more similar and closer to the ones in Fig. 3.



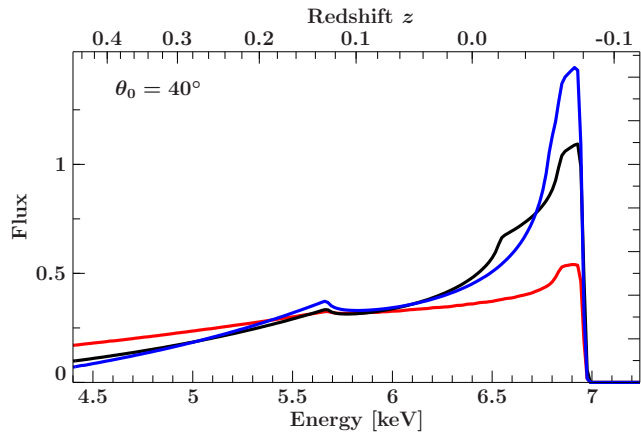


**Figure 5.** A broadened emission line with  $E_0 = 6.4$  keV for different spins of the black hole, emerging from an accretion disc which is assumed to extend down to the marginal stable radius. Common parameters were chosen for the inclination angle ( $\theta_0 = 40^\circ$ ) and the emissivity ( $r^{-3}$ ). The color code is that of Fig. 3, i.e.,  $a = +0.998$  is drawn in red (dashed),  $a = 0$  in black (dashed-dotted), and  $a = -0.998$  in blue (solid).

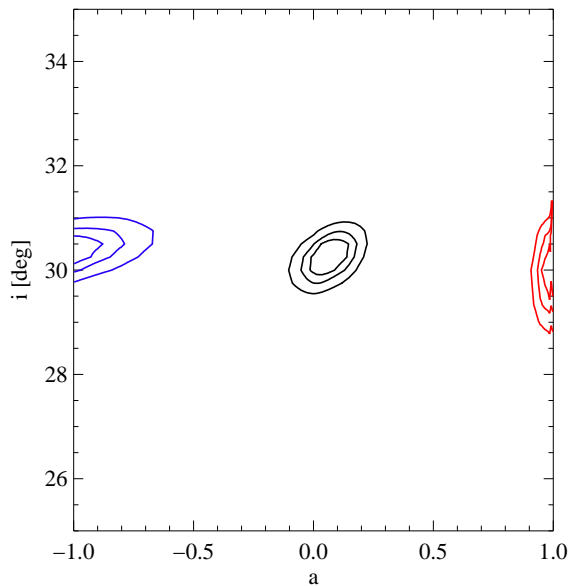


**Figure 6.** Confidence contours for simulated 50ksec observations of MCG-6-30-15 with IXO. Confidence contours at 68%, 90% and 99% confidence are shown for three simulations assuming  $a = -0.998$ ,  $a = 0$ , and  $a = +0.998$ , respectively. In the determination of the contours, the continuum parameters ( $N_H$ ,  $\Gamma$ , and continuum normalization) and the line energy were left free.

In order to study the question of observability in greater detail, we have performed simulations of observations of a relativistic line with the planned International X-ray Observatory (IXO), using response matrices obtained from the IXO team (Smith, priv. comm.). We base the simulations on power-law fits to *XMM-Newton* data from MCG-6-30-15 in a typical state, using a power law continuum with a 2–10 keV flux of  $2.5 \times 10^{-11}$  erg cm $^{-2}$  s $^{-1}$  and photon index  $\Gamma = 1.6$ , absorbed by a column  $N_H = 10^{21}$  cm $^{-2}$ . We set the equivalence width of the line to 350 eV (typical for MCG-6-30-15). Figure 6 shows that in a 50 ksec observation the next gen-

eration X-ray instrumentation will easily allow to separate even the difficult case of negatively spinning black holes.

In summary, motivated by predictions of negatively spinning black holes from cosmology and from birth scenarios for Galactic black holes (Brandt & Podsiadlowski 1995; Volonteri et al. 2005; King et al. 2008), we have presented new results on the shape of relativistic lines from accretion discs around black holes for the case that the angular momenta of the disc and the black hole are aligned and counter-aligned (King et al. 2005). We have shown that lines from counterrotating discs are narrower than those from Schwarzschild black holes, since the marginally stable orbit moves outwards as the black hole’s angular momentum decreases. Since these lines still have a slight asymmetric shape, we still expect them to be observable. We have also presented a new and more flexible scheme for the calculation of line profiles for black holes of all possible angular momenta and for arbitrary emissivity and limb-darkening laws, which has a significantly smaller footprint in terms of the amount of precalculation required. The model is available from [www.sternwarte.uni-erlangen.de/research/relline/](http://www.sternwarte.uni-erlangen.de/research/relline/). Comparison of the model shows that for the case  $a \geq 0$  its results are in agreement with the modern relativistic line model of Dovčiak et al. (2004).

*Acknowledgments.* We acknowledge partial support from the European Commission under contract ITN 215212 “Black Hole Universe”. We thank John Davis for the development of the `SLxFig` module used to prepare the figures in this paper and Manfred Hanke and Roland Speith for useful comments. We thank the referee for insightful comments that significantly improved the paper.

## REFERENCES

- Arnaud K. A., 1996, in G. H. Jacoby & J. Barnes ed., *Astronomical Data Analysis Software and Systems V* Vol. 101 of *Astronomical Society of the Pacific Conference Series*, XSPEC: The First Ten Years. pp 17–†
- Bardeen J. M., Press W. H., Teukolsky S. A., 1972, *ApJ*, 178, 347
- Blum J. L., Miller J. M., Fabian A. C., Miller M. C., Homan J., van der Klis M., Cackett E. M., Reis R. C., 2009, *ApJ*, 706, 60
- Boyer R. H., Lindquist R. W., 1967, *Journal of Mathematical Physics*, 8, 265
- Brandt N., Podsiadlowski P., 1995, *MNRAS*, 274, 461
- Brenneman L. W., Reynolds C. S., 2006, *ApJ*, 652, 1028
- Caballero-García M. D., Miller J. M., Díaz Trigo M., Kuulkers E., Fabian A. C., Mas-Hesse J. M., Steeghs D., van der Klis M., 2009, *ApJ*, 692, 1339
- Cackett E. M., Miller J. M., Bhattacharyya S., Grindlay J. E., Homan J., van der Klis M., Miller M. C., Strohmayer T. E., Wijnands R., 2008, *ApJ*, 674, 415
- Cackett E. M., Miller J. M., Homan J., van der Klis M., Lewin W. H. G., Méndez M., Raymond J., Steeghs D., Wijnands R., 2009, *ApJ*, 690, 1847
- Carter B., 1968, *Phys. Rev.*, 174, 1559
- Comastri A., Brusa M., Civano F., 2004, *MNRAS*, 351, L9
- Corral A., Page M. J., Carrera F. J., Barcons X., Mateos S., Ebrero J., Krumpke M., Schwöpe A., Tedds J. A., Watson M. G., 2008, *A&A*, 492, 71
- Cunningham C. T., 1975, *ApJ*, 202, 788
- Cunningham J. M., Bardeen C. T., 1973, *ApJ*, 183, 237
- di Salvo T., D’Af A., Iaria R., Burderi L., Dovčiak M., Karas V.,

- Matt G., Papitto A., Piraino S., Riggio A., Robba N. R., Santangelo A., 2009, *MNRAS*, 398, 2022
- Done C., Diaz Trigo M., 2010, *MNRAS*, pp 1097–+
- Dovčiak M., Karas V., Yaqoob T., 2004, *Astrophysical Journal Supplement*, 153, 205
- Fabian A. C., Rees M. J., Stella L., White N. E., 1989, *MNRAS*, 238, 729
- Fabian A. C., Sanders J. S., Etori S., Taylor G. B., Allen S. W., Crawford C. S., Iwasawa K., Johnstone R. M., Ogle P. M., 2000, *MNRAS*, 318, L65
- Fabian A. C., Zoghbi A., Ross R. R., Uttley P., Gallo L. C., Brandt W. N., Blustin A. J., Boller T., Caballero-Garcia M. D., Larsson J., Miller J. M., Miniutti G., Ponti G., Reis R. C., Reynolds C. S., Tanaka Y., Young A. J., 2009, *Nat*, 459, 540
- Garofalo D., 2009, *ApJ*, 699, 400
- Garofalo D., Evans D. A., Sambruna R. M., 2010, *MNRAS*, 406, 975
- Haardt F., 1993, *ApJ*, 413, 680
- Houck J. C., Denicola L. A., 2000, in Manset N., Veillet C., Crabtree D., eds, *Astronomical Data Analysis Software and Systems IX* No. 216 in *ASP Conf. Ser.*, Isis: An interactive spectral interpretation system for high resolution x-ray spectroscopy. p. 591
- Jaroszynski M., 1997, *Acta Astronomica*, 47, 399
- Kataoka J., Reeves J. N., Iwasawa K., Markowitz A. G., Mushotzky R. F., Arimoto M., Takahashi T., Tsubuku Y., Ushio M., Watanabe S., Gallo L. C., Madejski G. M., Terashima Y., Isobe N., Tashiro M. S., Kohmura T., 2007, *PASJ*, 59, 279
- Kerr R. P., 1963, *Phys. Rev. Lett.*, 11, 237
- King A. R., Lubow S. H., Ogilvie G. I., Pringle J. E., 2005, *MNRAS*, 363, 49
- King A. R., Pringle J. E., Hofmann J. A., 2008, *MNRAS*, 385, 1621
- Krolik J. H., 1999, *Active galactic nuclei: from the central black hole to the galactic environment*. Princeton Univ. Press, Princeton
- Laor A., 1991, *ApJ*, 376, 90
- Lindquist R. W., 1966, *Annals of Physics*, 37, 487
- Longinotti A. L., de La Calle I., Bianchi S., Guainazzi M., Dovčiak M., 2008, *Memorie della Societa Astronomica Italiana*, 79, 259
- Martocchia A., Matt G., Karas V., Belloni T., Feroci M., 2002, *A&A*, 387, 215
- Miller J. M., Fabian A. C., Reynolds C. S., Nowak M. A., Homan J., Freyberg M. J., Ehle M., Belloni T., Wijnands R., van der Klis M., Charles P. A., Lewin W. H. G., 2004, *ApJ*, 606, L131
- Miller J. M., Fabian A. C., Wijnands R., Remillard R. A., Wondolowski P., Schulz N. S., Di Matteo T., Marshall H. L., Canizares C. R., Pooley D., Lewin W. H. G., 2002, *ApJ*, 578, 348
- Miller J. M., Reynolds C. S., Fabian A. C., Cackett E. M., Miniutti G., Raymond J., Steeghs D., Reis R., Homan J., 2008, *ApJ*, 679, L113
- Miller J. M., Reynolds C. S., Fabian A. C., Miniutti G., Gallo L. C., 2009, *ApJ*, 697, 900
- Miniutti G., Fabian A. C., Anabuki N., Crummy J., Fukazawa Y., Gallo L., Haba Y., Hayashida K., Holt S., Kunieda H., et al., 2007, *PASJ*, 59, 315
- Nandra K., O’Neill P. M., George I. M., Reeves J. N., 2007, *MNRAS*, 382, 194
- Reynolds C. S., Fabian A. C., 2008, *ApJ*, 675, 1048
- Reynolds C. S., Garofalo D., Begelman M. C., 2006, *ApJ*, 651, 1023
- Reynolds C. S., Nowak M. A., 2003, *Phys. Rep.*, 377, 389
- Ross R. R., Fabian A. C., 2007, *MNRAS*, 381, 1697
- Schnittman J. D., 2006, *ArXiv Astrophysics e-prints*
- Shaposhnikov N., Titarchuk L., Laurent P., 2009, *ApJ*, 699, 1223
- Speith R., Riffert H., Ruder H., 1995, *Computer Physics Communications*, 88, 109
- Streblyanska A., Hasinger G., Finoguenov A., Barcons X., Mateos S., Fabian A. C., 2005, *A&A*, 432, 395
- Svoboda J., Dovčiak M., Goosmann R., Karas V., 2009, *A&A*, 507, 1
- Tanaka Y., Nandra K., Fabian A. C., Inoue H., Otani C., Dotani T., Hayashida K., Iwasawa K., Kii T., Kunieda H., Makino F., Matsuoka M., 1995, *Nat*, 375, 659
- Thorne K. S., 1974, *ApJ*, 191, 507
- Volonteri M., Madau P., Quataert E., Rees M. J., 2005, *ApJ*, 620, 69
- Wilms J., Reynolds C. S., Begelman M. C., Reeves J., Molendi S., Staubert R., Kendziorra E., 2001, *MNRAS*, 328, L27
- Wise M. W., McNamara B. R., Nulsen P. E. J., Houck J. C., David L. P., 2007, *ApJ*, 659, 1153
- Yamada S., Makishima K., Uehara Y., Nakazawa K., Takahashi H., Dotani T., Ueda Y., Ebisawa K., Kubota A., Gandhi P., 2009, *ApJ*, 707, L109